Observation of plasma confinement in picosecond laser-plasma interactions

A. R. Bell,[1] F. N. Beg,[1] Z. Chang,[2] A. E. Dangor,[1] C. N. Danson,[2] C. B. Edwards,[2] A. P. Fews,[3] M. H. R. Hutchinson,[1] S. Luan,[1] P. Lee,[1] P. A. Norreys,[2] R. A. Smith,[1] P. F. Taday,[2] and F. Zhou[1]
[1]*Imperial College of Science and Technology, Prince Consort Road, London SW7 2AZ, United Kingdom*
[2]*SERC Rutherford Apppleton Laboratory, Chilton, Didcot, Oxon OX11 0QX, United Kingdom*
[3]*H. H. Wills Physics Laboratory, University of Bristol, Royal Fort, Tyndall Avenue, Bristol BS8 1TL, United Kingdom*
(Received 6 May 1993)

Novel features associated with multiterawatt laser interactions with solid targets at incident irradiances in the range $(1.0–12.0)\times 10^{17}$ W cm^{-2} are presented. Collimation of the plasma flow normal to the target surface has been observed in time-integrated x-ray images and ion-velocity measurements. Ions emitted from the target have a characteristic energy of typically 100 keV. The ion spectrum extends to 1.5 MeV. Calculations are presented that suggest the observed collimation is due to a large magnetic field pinching the plasma.

PACS number(s): 52.50.Jm

I. INTRODUCTION

Laser-plasma interactions have been extensively studied under conditions where the laser pulse length is long enough to allow the hydrodynamic flow of the plasma to approach a steady state and where heating occurs at densities close to the critical density [1]. Energetic ion emission has long been observed under such conditions, especially at high irradiance [2]. However, few studies have been performed under conditions where the laser pulse is short compared with the hydrodynamic response time of the plasma and where heating occurs close to solid density [3–9]. Interesting new areas of physics have now been opened up with the capability of focusing picosecond, multiterawatt-powered pulses in near-diffraction limited spots as it is now possible to achieve irradiances previously inaccessible in the laboratory. These new areas include such fields as short-wavelength x-ray lasers [10] and wake-field acceleration [11]. A number of articles exist that review these new fields [12]. The intrinsic interest in the response of the plasma to laser intensities as high as 10^{18} W cm^{-2} under short (picosecond) pulse conditions led us to conduct an experiment on the Nd-glass laser VULCAN at the Central Laser Facility of the Rutherford Appleton Laboratory.

In the experiment reported here, laser pulses of up to 30 J in pulses of 2.1 psec or longer were incident on a number of different target materials in a focal spot of ~ 50 μm with a measured contrast ratio of better than 10^{-6}. We present time-integrated x-ray images that show that the plasma flow is collimated normal to the target surface. Ion-velocity measurements reveal that most of the energy associated with the ions is carried by ions ≥ 100 keV/nucleon. The ion spectrum extends up to 1.5 MeV. CR-39 detectors reveal that most of the high-energy ions are protons, consistent with other previously reported experiments. Those ions with energy ≥ 100 keV are confined to a half-angle 10° cone, which is further strong evidence of a collimated plasma flow. The observations are supported by numerical calculations that suggest that the plasma flow may be collimated due to an azimuthal magnetic field pinching the plasma.

II. EXPERIMENT

Laser pulses were generated using the Nd glass laser VULCAN, which was equipped a chirped-pulse amplification (CPA) system. This consisted of an additive pulse mode-locked oscillator that provided pulses of 2.5 psec of 3 nJ energy and wavelength 1.053 μm. This pulse was then temporally expanded in a grating pair stretcher to 80 psec and amplified in the laser chain. The pulse was then recompressed by a second pair of diffraction gratings of this pair was located inside the target chamber under vacuum. The recompressed beam of diameter 140×88 mm^2 was then projected onto a partially reflecting turning mirror that allowed 5% of the recompressed pulse through for measurements of the laser pulse length, prepulse, spectral distribution and focal spot aberrations. An off-axis parabolic mirror located 44 cm from the target then focused the laser beam onto the target. A diagram of the compression chamber and the focusing arrangement is shown in Fig. 1. Approximately half of the laser energy was incident onto the target in a focal spot of 15×50 μm^2 (as measured by the equivalent plane monitor).

A full description of the laser system has been given elsewhere [13]. The important parameters of the laser system are as follows: up to 30 J of laser energy was incident on the target; the pulse length ranged from 2.1 to 7.5 psec; 90% of the laser energy was focused by the off-axis paraboloid mirror through a 100-μm pinhole; the incident irradiance on the target varied from 1.0×10^{17} to 12.0×10^{17} W cm^{-2}; the beam was p polarized and was incident on the target at an angle of 30° to the target normal. The prepulse was measured by both a cross correlator and an autocorrelator to be less than 10^{-6} of the main pulse intensity [13].

A variety of different targets were irradiated. These were plastic (Mylar), carbon (graphite), copper, and gold.

They consisted of either solid slabs of material or small "lollipop" disks 270 μm thick in diameter and 10 μm thick for gold and copper and 50 μm for Mylar. The laser beam was at 30° to the target normal. This was for two reasons: first, to eliminate as much backscattered radiation from the target as possible to protect the laser chain, and second, to ensure that there was some resonance absorption.

Four diagnostics were employed to measure the plasma parameters. The first was a pair of pinhole cameras to image the plasma that was created. Both cameras were situated 37° in the vertical direction from the horizontal plane and at 11° and 35° to the target normal (called cameras *A* and *B* for brevity). The positions of these cameras are shown in Fig. 1. Both cameras had 10-μm pinholes in 100-μm platinum substrates. The magnifications were $\times 16$ and $\times 11$, giving spatial resolutions of 11 and 12 μm for cameras *A* and *B*, respectively. They were filtered differently from shot to shot, depending on the target material that was being irradiated. All images were recorded on Kodak DEF film. The γ curves for the different x-ray wavelengths were taken from Ref. 14.

Two diagnostics were used to monitor the ion velocity from the plasma. CR-39 nuclear plastic track detectors [15] of dimension 2.5 cm^2 were used to monitor particles with energies >75 keV/nucleon. These detectors also gave quantitative information on the ion species, energy distribution, total number of particles incident on the detector, and the angular distribution of the particles around the axis normal to the target. In all shots one piece of CR-39 detector was placed at normal incidence (at a distance of 3.0 m from the target), and two pieces were placed in the horizontal plane at 45° and 75° to the target normal on the chamber wall at a distance of 46 cm. A Mylar filter array consisting of eight steps of 2 μm of Mylar was placed in front of each detector. On some shots, two additional detectors were placed at 20° and 60° to the target normal.

The second diagnostic to monitor the ions was an array of Faraday cups. These cups were of a conventional design with a honeycomb collecting electrode to reduce secondary-electron emission [16] and were biased at about 150 V to separate the neutralizing electron from the collecting ions. This sets the upper detectable ion energy at 300 keV/nucleon with decreasing sensitivity above 100 keV/nucleon. The cups were positioned at the chamber wall at a distance of 41 cm from the plasma. The signals were detected on a multichannel Hewlett-Packard digitizing oscilloscope with a time resolution of 5 nsec.

Finally, two NaI scintillators coupled to photomultiplier detectors were used to detect and measure the hard-x-ray emission. The detectors were placed outside the target chamber at a distance of 60 cm from the target behind an entrance port fitted with 15 mm of aluminum plate. Some information about the energy distribution was obtained by using a lead filter (which varied from 2 to 4 mm thick) in front of one of the detectors; the other detector was not filtered.

III. RESULTS

The pinhole cameras show clearly that in nearly all high-energy laser shots there is a collimated plume of plasma flowing from the target in the direction normal to the target surface. This can be seen in Fig. 2 which shows x-ray images obtained in a number of different shots (except the 15-J 3.5-psec shot on copper images, which is the same shot but viewed from different directions). The laser parameters for each shot are listed under each image, as is the filtering used. Two x-ray filters were used: 1 μm of nickel for mylar targets and 5 μm of tantalum for copper and gold targets. These gave a 50% transmission of x rays at 3.0 and 19.0 keV for the Ni and Ta filters, respectively. The pulse length quoted was that obtained from the single-shot autocorrelator. In those cases where only an estimate of the pulse length is given in Fig. 2, the pulse length was taken from shots fired under similar conditions (i.e., similar energy and *B* integral). The plasma plumes can clearly be seen in all the shots. The longest plume length was 240 μm for a gold target with a 15-J 2.3-psec shot.

It is possible to distinguish between the heated plasma on the target surrounding the focused laser spot and the collimated plasma plume flowing along the target normal due to the oblique angle of the pinhole cameras. Figure 3 shows the full width at half maximum (FWHM) of the x-ray images of the heated plasma at the target surface (measured in the vertical dimension of the incident laser beam). It should be noted that different filters were used for different target materials. Nevertheless, it appears from Fig. 3 that the target plasma surrounding the laser

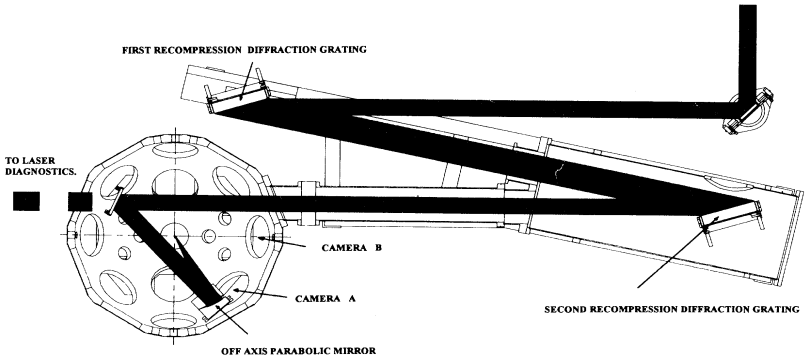

FIG. 1. Schematic outline of the CPA chamber and focusing optics.

focal spot increases with increasing incident laser energy. The equivalent plane monitor showed that the focal spot had a vertical dimension of 15 μm, the horizontal being 50 μm. It was found from the x-ray images that the vertical dimension was never less than 60 μm. The vertical-to-horizontal dimensions of the heated regions were in the ratio 2:3. This suggests that the increase in the "focal spot" is due to radiation and/or electron energy transport and is not a laser (i.e., B-integral) effect.

Figure 4 shows the energy spectrum for ions >100 keV for a CR-39 detector placed at zero angle to the target normal when a laser pulse of energy 17.3 J and pulse length 3.0 psec was projected onto a Mylar lollipop target. The spectrum in the 100–700-keV region was found by counting the particle tracks in the different Mylar layers (as the track density was too high for detailed spectroscopy). The spectrum in the 0.7–1.5-MeV range was analyzed by a measurement of individual particle tracks. The count is per 20-keV energy bin. The number of tracks in both regimes was counted over a solid angle of 10^{-7} sr.

Where detailed spectroscopy was possible, it was found that on all shots of any type of target material the particles were protons. This observation that the fastest ions are protons, even for nonhydrogenic targets, is consistent with previous experiments [17], where they are presumed to be associated with hydrocarbon contamination of the target surface and with theory [18] which shows that lighter ions are accelerated to higher speeds.

Clearly, Fig. 4 suggests that there is a peak in the spectrum at 300–400 keV, after which there is an exponentially decaying tail. Particles up to 1.5 MeV were detected. The broad peak and exponential tail were observed in all shots. By fitting an $\exp(-E/kT)$ curve to the exponentially decaying tail, a best-fit ion temperature of 200 keV was fitted for this particular shot. The measured ion temperatures were in the range 100–200 keV.

The hard-x-ray NaI photomultiplier detectors indicated the existence of fast electrons. Assuming that the emission is bremsstrahlung from the fast electrons and can be described by a $\exp(-E/kT)$ profile, the measured intensities of the two hard-x-ray detectors are consistent with an electron temperature of around 300 keV.

The Faraday cups were not calibrated, so it is not possible to gain any information from them about collimation. The main information they give is about the ion velocity spectrum. Figure 5 shows two graphs of the integrated energy spectrum (total energy arriving at the cups of ions with energy greater than E eV/nucleon) for cups placed at 10° and 22°, respectively from the target normal for a 19.0-J 2.4-psec shot onto copper. It is clear from the velocity spectrum in Fig. 5 that most of the energy comes off in ions with energy per nucleon ~ 100 keV, even though the sensitivity of Faraday cups falls at this energy due to biasing voltage. These graphs show that the Faraday cups do not detect a significant amount of energy in a lower-energy "thermal" component. The angular flux of 100–300 keV ions detected by the CR-39 is shown in Fig. 6(a). It is clear that these ions are collimated into a half-angle cone of $\sim 10°$. Figure 6(b) shows the total flux of ions incident on the CR-39 detectors with angle. it shows that the integrated fast ion emission is rather broader and occupies a $\sim 20°$ half-angle cone. Clearly, these results confirm that the plasma blow-off is collimated about the target normal.

By knowing the number of ions, the solid angle of the detector, and the energy of the particles, it is now possible to estimate the absorbed laser energy. Assuming that there is symmetry about the target normal in the ion emission, and that all ions making tracks in the detectors were protons, then the energy absorption in the >100-keV range averaged $\sim 2\%$ of the incident energy and was

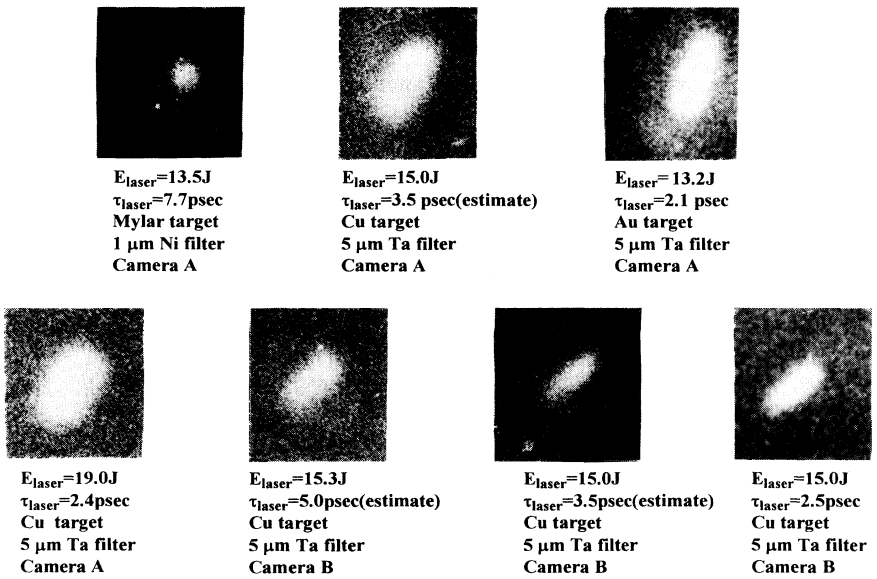

FIG. 2. X-ray images of picosecond high-intensity laser-produced plasmas. Target materials, laser energy, pulse length and x-ray filters for the shot are listed under each image.

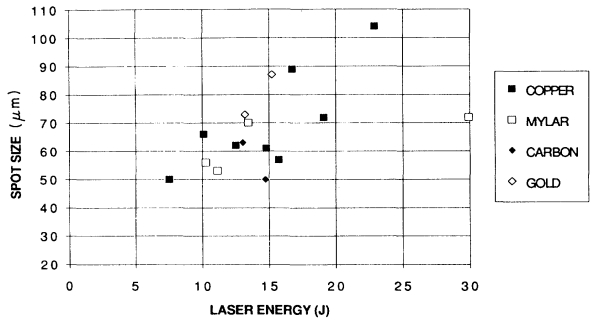

FIG. 3. Measured x-ray image FWHM of focal spot region plotted against incident laser energy.

never greater than ~5%. This absorption fraction in the fast ions did not appear to vary with target material and remained fairly constant over the range $(1.0-12.0)\times10^{17}$ W cm^{-2} incident irradiance.

IV. DISCUSSION

Ion emission from laser-irradiated solid targets can often be divided into (a) a thermal component with a velocity representative of the bulk sound speed in the target and (b) a high-energy component with an energy representative of the suprathermal electron temperature. Gitomer *et al.* [17] have compiled fast-ion data from experiments at many laboratories with a wide range of laser wavelengths and pulse lengths. At an irradiance of $I\lambda^2=2.0\times10^{17}$ W cm^{-2} their compiled data for the characteristic fast ion energy span the range 150 keV to 1 MeV. Our CR-39 detector data indicate an energy around 100 and 200 keV, which is at the lower end of this range. Our Faraday-cup data are consistent with this since most of the detected ion energy is carried by ions with energies around 100 keV despite the sensitivity of the cups falling rapidly at this energy due to the biasing. The Faraday cups do not detect a significant amount of energy in a lower energy thermal component. Two factors may explain this

(1) The electron thermalization time

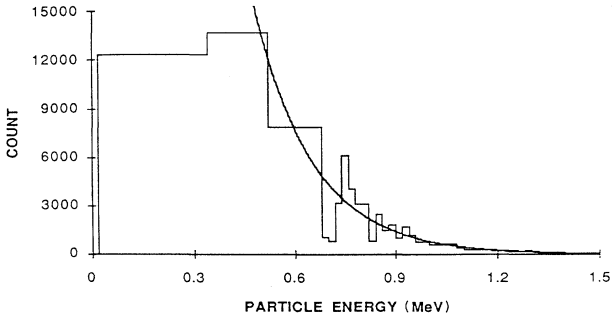

FIG. 4. Ion count plotted against energy. The CR-39 detector subtended 10^{-7} sr solid angle the target. A best-fit $\exp(-E/kT)$ temperature curve of 200 keV is shown.

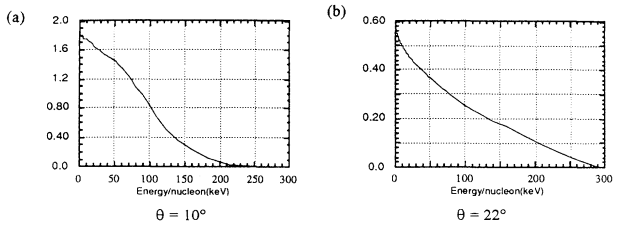

FIG. 5. Total energy arriving at the cups [ordinate (in arbitrary units)] plotted against ions with energy greater than E eV/nucleon (abscissa) for a Faraday cup placed at (a) 10° and (b) 22° to the target normal.

$$\tau_{ee}=7\left[\frac{kT}{100\text{ keV}}\right]^{3/2}\left[\frac{\ln\Lambda}{5}\right]^{-1}\left[\frac{n_e}{3\times10^{23}\text{ cm}^{-3}}\right]^{-1}\text{ psec} \quad (1)$$

is longer than the laser pulse length even at solid density and is very much longer at the critical density. Hence, a thermal electron component cannot develop during the laser pulse, and the plasma expansion is driven by energetic electrons if the expansion time is shorter than the thermalization time.

(2) The energy is absorbed in such a small region of space that the energy per particle has to be of the order of 100 keV. As suggested below, thermal conduction may be strongly inhibited by the presence of a magnetic field, in which case the absorbed energy could be confined to a thin surface layer and generate a very high temperature. If we suppose that the absorbed energy E_{abs} is contained within a cylinder that has the radius of the focal spot (25 μm) and extends a distance D into the target,

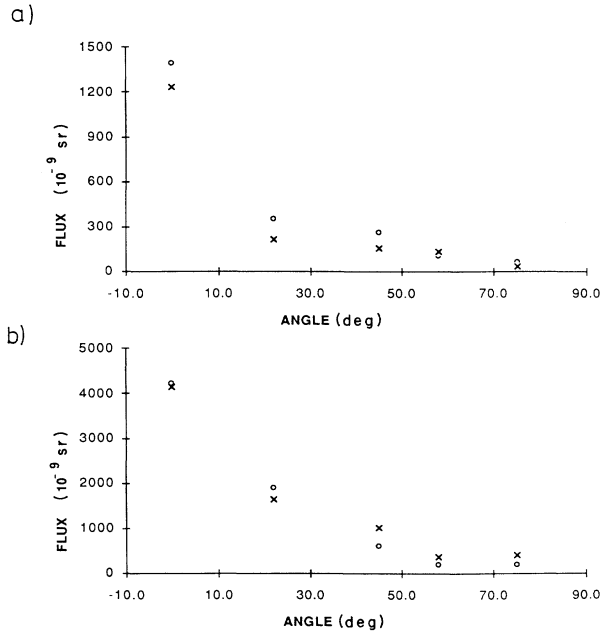

FIG. 6. Ion count from CR-39 detector in 10^{-9} sr solid angle plotted against angle to the target normal for two 20-J shots onto Cu targets for an energy range of (a) 100–300 keV, (b) total energy incident on the detector.

then this volume of plasma is heated to a temperature

$$kT = 1600 \left[\frac{E_{\text{abs}}}{3\ \text{J}}\right]\left[\frac{D}{1\ \mu\text{m}}\right]^{-1}\left[\frac{\bar{n}_e}{10^{21}\ \text{cm}^{-3}}\right]^{-1}$$
$$= 5 \left[\frac{E_{\text{abs}}}{3\ \text{J}}\right]\left[\frac{D}{1\ \mu\text{m}}\right]^{-1}\left[\frac{\bar{n}_e}{3\times 10^{23}\ \text{cm}^{-3}}\right]^{-1}\ \text{keV}\ , \tag{2}$$

where $\bar{n}_e$ is the average electron density in the cylinder.

Both CR-39 detector data and x-ray images indicate collimation of the out-flowing plasma. Ion collimation has previously been observed by Burgess, Luther-Davies, and Nugent [19] with a 2-J 20-psec laser pulse. Using ion calorimetry and interferometry, Burgess, Luther-Davies, and Nugent showed that fast ions were emitted within a 10° cone and all ions (fast and thermal) were collimated to a 25° cone.

Collimation of the very fastest ions may be explicable in terms of uniform acceleration by an electrostatic field [20] at the surface of the target while it is still relatively flat at the start of the expansion, but collimation of the majority of the ions cannot be explained in this way since their dynamics are more correctly described as a bulk expansion away from a point of origin (the laser spot). We suggest that the collimation observed in our experiment is caused by magnetic pinching. A magnetic field is generated by the pressure-driven source term $\partial B/\partial t = -\nabla\times(\nabla P/n_e e)$ (e.g., Stamper [21]) which is nonzero because the density and temperature gradients are not parallel. The density gradient is directed into the target, and the temperature gradient has a component along the target surface. A rough estimate is that $B \sim \tau L_T^{-1} L_n^{-1} kT/e$, where τ is the pulse length, L_T and L_n are the temperature and density scale lengths. Equivalently,

$$B \sim \left[\frac{\tau}{2\ \text{psec}}\right]\left[\frac{kT}{100\ \text{keV}}\right] \times \left[\frac{L_T}{25\ \mu\text{m}}\right]^{-1}\left[\frac{L_n}{1\ \mu\text{m}}\right]^{-1} 80\ \text{MG}\ . \tag{3}$$

This estimate neglects resistive and convective losses, which would reduce the field, and continued field generation after the end of the laser pulse, which would increase the field. This estimate indicates a plasma β of

$$\beta = \frac{P}{B^2/2\mu_0} \sim 0.6 \left[\frac{\tau}{2\ \text{psec}}\right]^{-2}\left[\frac{kT}{100\ \text{keV}}\right]^{-1} \times \left[\frac{L_T}{25\ \mu\text{m}}\right]^{2}\left[\frac{L_n}{1\ \mu\text{m}}\right]^{2}\left[\frac{n_e}{n_{\text{crit}}}\right]\ . \tag{4}$$

Within the uncertainties of the calculation, the magnetic and thermal pressures are comparable and the magnetic pressure may dominate in the underdense plasma. The magnetic field is azimuthal about the laser-beam axis. In this configuration it can act to pinch the plasma onto the axis, or at least constrain its lateral expansion during ablation. The thermal pressure can be expected to fall due to thermal conduction and radiation at the end of the laser pulse, thus enhancing the relative effect of the magnetic pressure, although this, too, will decay resistively. We suggest that it is this pinching that gives rise to the elongated plasma plume observed in the x-ray images and CR-39 data.

The magnetic field may also inhibit transport. The electron gyroradius is

$$r_g = 0.1 \left[\frac{kT}{100\ \text{keV}}\right]^{1/2}\left[\frac{B}{80\ \text{MG}}\right]^{-1}\ \mu\text{m}\ . \tag{5}$$

If moving sonically, the plasma expands about 5 μm during the laser pulse, which is greater than r_g. Hence, the magnetic field is capable of restricting energy transport away from the critical surface and laterally along the target surface. Using the above estimate of the field [Eq. (3)], the Hall parameter $\omega\tau_{ei}$ (where ω is the Larmor frequency and τ_{ei} is the electron-ion collision time) is

$$\omega\tau_{ei} \sim 8\times 10^5 \left[\frac{\tau}{2\ \text{psec}}\right]\left[\frac{kT}{100\ \text{keV}}\right]^{5/2}\left[\frac{Z}{4}\right]^{-1} \times \left[\frac{L_T}{25\ \mu\text{m}}\right]^{-1}\left[\frac{L_n}{1\ \mu\text{m}}\right]^{-1}\left[\frac{n_e}{n_{\text{crit}}}\right]^{-1}\ . \tag{6}$$

By a large margin this is sufficient to severely reduce energy transport from the laser spot. Even if the full Braginskii [22] reduction in conductivity [$\propto(\omega\tau_e)^{-2}$] is not achieved because the field is disordered or the gyroradius is not much less than the scale lengths, energy transport is clearly going to be inhibited. This supports the conclusion of Eq. (2) that the characteristic electron temperature may be very high.

Since the electron collision times are very long a particle description would be more appropriate. Particle simulations by Forslund and Brackbill [20] have shown that the magnetic field is important at high $I\lambda^2$. However, a fluid code describes the bulk properties adequately and is much more efficient computationally. The supposition that the plumes are collimated magnetically was investigated further with a computer code (MH2D) that solves the magnetohydrodynamic (MHD) equations in cylindrical (r,z) geometry. The code includes the pressure-driven source term, resistive diffusion of magnetic field, and Spitzer thermal conduction with magnetic inhibition. The plasma is treated as a single-temperature, fully ionized perfect gas. Laser energy is absorbed by a 20% dump at the critical surface into the thermal plasma. Electric currents are limited so that the electron drift velocity does not exceed the electron thermal velocity. Additional transport effects, such as Righi-Leduc and Nernst terms, are ignored. Transport by ions or suprathermal electrons are not included. Because many undeniably important effects are not included, our calculations cannot justifiably be called a "simulation." However, the limited physics included in the calculation probably causes less uncertainty that the effect of magnetic field on energy transport.

The code was run for a plastic foil irradiated by a 4-psec laser pulse at an irradiance of 3×10^{17} W cm^{-2} fo-

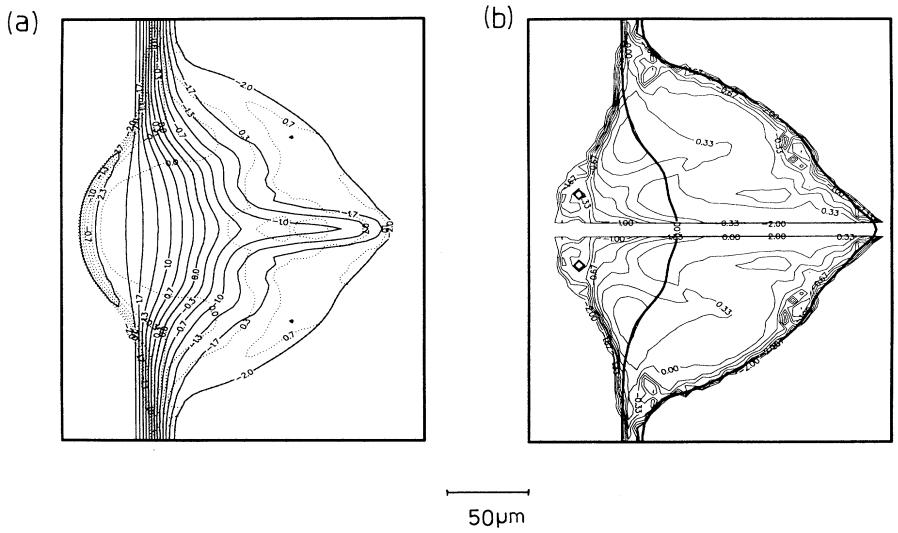

FIG. 7. Logarithmic contour plots of (a) density (in units of 10^{21} cm^{-3}) and temperature (keV) and (b) magnetic field (in MG) 28 psec after the peak of the laser pulse. The thick contour lines on (b) give the positions of the critical surface and the plasma-vacuum interface.

cused to a 50-μm-diameter spot. The density profile was initialized with an exponential ramp with an exp-folding distance of 2 μm. The ramp is necessary because the baroclinic source of the magnetic field is proportional to ∇n_e, which therefore cannot be allowed to be infinite. This is not a significant limitation because the foil expands through a large distance during the laser pulse. Magnetic inhibition of heat flow was imposed by reducing the Spitzer conductivity by $(\omega\tau_e)^{-3/2}$, where $\omega\tau_e$ is limited to a maximum value of 10^{-4}. This inhibition was preferred to the full Braginskii reduction $(\omega\tau_e)^{-2}$ which, when applied, produced maximum temperatures of around 1 MeV by virtually halting energy transport from the critical surface. While being within the range of temperatures estimated above [Eq. (5)], 1 MeV clearly disagrees with the data. Experimentally, transport inhibition is probably weakened by disorder in the magnetic field and by the Larmor radius being not much smaller than typical scale lengths. At the opposite extreme, the still weaker Bohm-like transport $(\omega\tau_e)^{-1}$ reduction was also tried but this resulted in temperatures much lower than indicated by the data. An $(\omega\tau_e)^{-3/2}$ reduction in transport gives a plasma temperature which is typically tens of keV and reaches a maximum of 130 keV at the peak of the laser pulse at the critical surface on the beam axis.

Before the laser intensity reaches its peak, transport is unmagnetized, and energy spreads easily along the target surface beyond the edge of the laser spot. But, as the magnetic field grows, $\omega\tau_e$ reaches a critical magnitude, at which point transport becomes inhibited, energy cannot escape from the laser spot, the peak temperature rises, the temperature gradient increases, and the magnetic field is produced more rapidly. This positive feedback causes a rapid rise in temperature and magnetic field. This effect has been seen previously in calculations of Yabe and Hasegawa [23]. The magnetic field reaches a peak value of 30 MG. The magnetic pressure of 40 Mbar plays a part in driving the ablation as previously noted by Craxton and Haines [24]. As an indication that our results are not extreme, we note that Wilks *et al.* [25], using a particle-in-cell code, albeit at an irradiance 10 times larger, find magnetic fields of 250 MG and magnetic pressures of 2500 Mbar.

Figure 7 presents logarithmic contour plots of calculated density, temperature, and magnetic field 30 psec after the peak of the laser pulse. The surface plasma is freely away from the target and is clearly collimated into a jet. The length of the jet is approximately 100 μm. Its temperature is 10 keV. Collimation was not observed when magnetic-field generation was omitted from the calculation.

The calculations that we have performed demonstrate that a magnetic field can grow to tens of MG, at which magnitude it strongly inhibits electron transport and causes the electron temperature to rise. The calculation also supports our suggestion that the jets are collimated by magnetic field, but here we have to be more cautious in our conclusions. By varying the magnetic transport inhibition between Braginskii and Bohm-like, the temperature can be made to vary by two orders of magnitude. Calculations with Braginskii inhibition showed much weaker collimation, and calculations with Bohm-like inhibition showed no collimation. Hence, we cannot conclude that collimation is a definite feature of short-pulse high-intensity experiments. Nevertheless, our results show that the observed collimation can be reproduced in numerical calculations that include magnetic pinching. We note that magnetic collimation might also play an important role in the production of jets during

the early stages of longer pulses when the target is irradiated with a laser beam containing small-scale hot spots [26].

V. CONCLUSION

We have reported novel features associated with the multiterawatt, picosecond laser interactions with solid targets for incident irradiances $(1.0\text{–}12.0)\times10^{17}$ W cm^{-2}. Plasma collimation has been conclusively observed in time-integrated x-ray images. Ion emission observed with faraday cups show no evidence of a significant low-energy component and most of the laser energy is carried with ions $\sim$100 keV/nucleon. The CR-39 detectors revealed that most of the high-energy particles were protons. The angular distribution of ions with energy of 100 keV have been shown to be confined to a 10° half-angle cone, which is further strong evidence of plasma collimation. It has been shown experimentally that ions with an energy $\geq$100 keV absorbed on average 2% (and never greater than 5%) of the incident laser energy. Our calculations suggest that magnetic collimation therefore seems a likely explanation of the plumes seen in the x-ray images and the evidence of collimation in the CR-39 data.

ACKNOWLEDGMENTS

The authors would like to thank the VULCAN laser operations, the target preparation, and the engineering groups of the Central Laser Facility for their assistance in carrying out this work. This work was supported by a collaborative program between the Imperial College of Science, Technology and Medicine London, the University of Southampton, and the Central Laser Facility of the Rutherford Appleton Laboratory. The work was funded by the Science board of U.K. Science and Engineering Research Council.

[1] M. H. Key, W. T. Toner, T. J. Goldsack, J. D. Kilkenny, S. A. Veats, P. F. Cunningham, and C. L. S. Lewis, Phys. Fluids **26**, 2011 (1983).
[2] W. C. Mead, R. A. Haas, W. L. Kruer, D. W. Phillion, H. N. Kornblum, J. D. Lindl, D. R. MacQuigg, and V. C. Rupert, Phys. Rev. Lett. **37**, 489 (1976).
[3] U. Tuebner, G. Kuhnle, and F. P. Schafer, Appl. Phys. Lett. **59**, 2672 (1991); Appl. Phys. B **54**, 493 (1992).
[4] M. M. Murnane, H. C. Kapteyn, M. D. Rosen, and R. W. Falcone, Science **251**, 531 (1991); M. M. Murnane, H. C. Kapteyn, and R. W. Falcone, Phys. Fluids B **8**, 2409 (1991).
[5] P. Audebert, J. P. Geindre, J. C. Gauthier, A. Mysyrowicz, J. P. Chambaret, and A. Antonetti, Europhys. Lett. **19**, 189 (1992).
[6] M. Chaker, J. C. Keiffer, J. P. Matte, H. Pepin, P. Audebert, P. Maine, D. Strickland, P. Bado, and G. Mourou, Phys. Fluids B **3**, 167 (1991).
[7] O. L. Landen and W. E. Alley, Phys. Rev. A **46**, 5089 (1992).
[8] R. Fedosejevs, R. Ottmann, R. Sigel, G. Kuhnle, S. Szatmari, and F. P. Schafer, Phys. Rev. Lett. **64**, 1250 (1990).
[9] J. A. Cobble, G. A. Kyrala, A. A. Hauer, A. J. Taylor, C. C. Gomez, N. D. Delamatar, and G. T. Schappert, Phys. Rev. A **39**, 454 (1989).
[10] N. H. Burnett and P. Corkhum, J. Opt. Soc. Am. B **6**, 1195 (1989).
[11] T. Tajima and J. M. Dawson, Phys. Rev. Lett. **43**, 267 (1979).
[12] T. C. Katsouleas, W. B. Mori, J. M. Dawson, and S. C. Wilks, Proc. SPIE **1229**, 98 (1990); D. C. Eder, P. Amendt, P. R. Bolton, G. Guethlein, R. A. London, M. D. Rosen, and S. C. Wilks, in *X-Ray Lasers 1992,* Proceedings of the 3rd International Colloqium on X-ray Lasers, edited by E. E. Fill, IOP Conf. Series No. 125 (Institute of Physics, Bristol, England, London, 1992).
[13] C. N. Danson, L. Barzanti, A. Damerell, M. D. Dooley, C. B. Edwards, S. Hancock, M. H. Key, R. Mahadeo, M. R. G. Miller, P. Norreys, C. E. Ollman, D. A. Pepler, D. A. Rodkiss, I. Ross, M. A. Smith, P. F. Taday, W. T. Toner, K. Wigmore, T. B. Winstone, R. W. W. Wyatt, Z. Chang, F. Beg, A. Bell, A. E. Dangor, M. H. R. Hutchinson, P. Lee, S. Luan, I. P. Mercer, R. A. Smith, and F. Zhou Proc. SPIE (to be published).
[14] S. L. Niffikeer, Ph.D. thesis, University of London, 1991.
[15] A. P. Fews and D. L. Henshaw, Nucl. Instrum. Methods **197**, 517 (1982); A. P. Fews, Nucl. Instrum. Methods B **71**, 465 (1992); **72**, 91 (1992).
[16] A. Raven, P. T. Rumsby, and J. Watson, Rev. Sci. Instrum. **51**, 351 (1980).
[17] S. J. Gitomer, R. D. Jones, F. Begay, A. W. Ehler, J. F. Kephart, and R. Kristal, Phys. Fluids **29**, 2679 (1986).
[18] L. M. Wickens, and J. E. Allen, Phys. Fluids **24**, 1894 (1981).
[19] M. D. J. Burgess, B. Luther-Davies, and K. A. Nugent, Phys. Fluids **28**, 2286 (1985).
[20] D. W. Forslund, and J. U. Brackbill, Phys. Rev. Lett. **48**, 1614 (1982).
[21] J. A. Stamper, Laser Part. Beams **9**, 841 (1991).
[22] S. I. Braginskii, in *Reviews of Plasma Physics,* edited by M. A. Leontovich (Consultants Bureau, New York, 1965), Vol. 1, p. 205.
[23] T. Yabe, and M. Hasegawa, Phys. Rev. Lett. **57**, 2667 (1986).
[24] R. S. Craxton and M. G. Haines, Plasma Phys. **20**, 487 (1978).
[25] S. C. Wilks, W. L. Kruer, M. Tabak, and A. B. Langdon, Phys. Rev. Lett. **69**, 1383 (1992).
[26] M. Desselberger, T. Afshar-rad, F. Khattak, S. Vianna, and O. Willi, Phys. Rev. Lett. **68**, 1539 (1992).

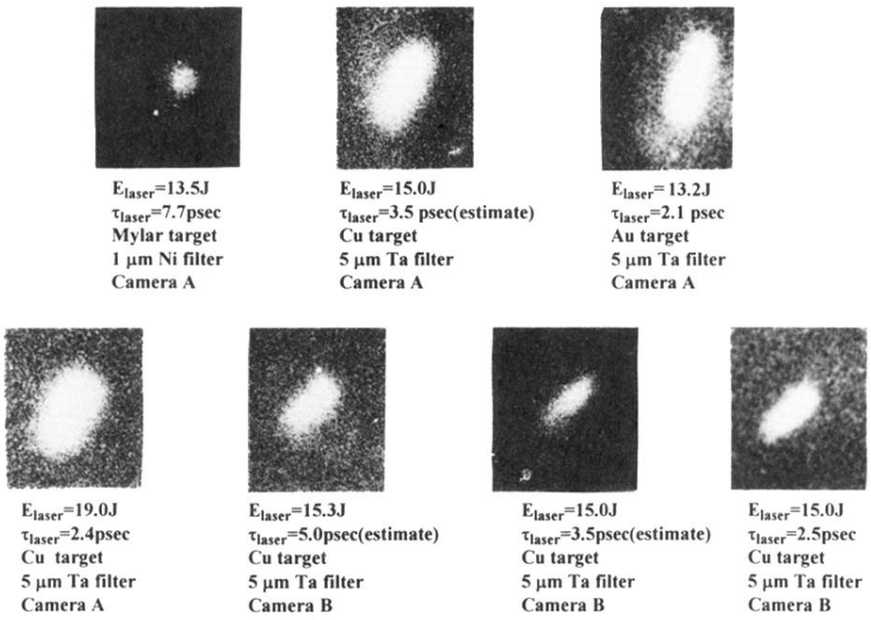

FIG. 2. X-ray images of picosecond high-intensity laser-produced plasmas. Target materials, laser energy, pulse length and x-ray filters for the shot are listed under each image.